Endosome-ER Contacts Control Actin Nucleation and Retromer Function through VAP-Dependent Regulation of PI4P

Rui Dong[1,2,3,5], **Yasunori Saheki**[1,2,3,5,7], **Sharan Swarup**[6], **Louise Lucast**[1,2,3,5], **J. Wade Harper**[6], and **Pietro De Camilli**[1,2,3,4,5,*]

[1]Department of Neuroscience, Yale University School of Medicine, New Haven, CT 06510, USA

[2]Department of Cell Biology, Yale University School of Medicine, New Haven, CT 06510, USA

[3]Howard Hughes Medical Institute, Yale University School of Medicine, New Haven, CT 06510, USA

[4]Kavli Institute for Neurosciences, Yale University School of Medicine, New Haven, CT 06510, USA

[5]Program in Cellular Neuroscience, Neurodegeneration and Repair, Yale University School of Medicine, New Haven, CT 06510, USA

[6]Department of Cell Biology, Harvard Medical School, Boston, MA 02115, USA

SUMMARY

VAP (VAPA and VAPB) is an evolutionarily conserved endoplasmic reticulum (ER)-anchored protein that helps generate tethers between the ER and other membranes through which lipids are exchanged across adjacent bilayers. Here, we report that by regulating PI4P levels on endosomes, VAP affects WASH-dependent actin nucleation on these organ-elles and the function of the retromer, a protein coat responsible for endosome-to-Golgi traffic. VAP is recruited to retromer budding sites on endosomes via an interaction with the retromer SNX2 subunit. Cells lacking VAP accumulate high levels of PI4P, actin comets, and *trans*-Golgi proteins on endosomes. Such defects are mimicked by downregulation of OSBP, a VAP interactor and PI4P transporter that participates in VAP-dependent ER-endosomes tethers. These results reveal a role of PI4P in retromer-/WASH-dependent budding from endosomes. Collectively, our data show how the ER can control budding dynamics and association with the cyto-skeleton of another membrane by direct contacts leading to bilayer lipid modifications.

Graphical abstract

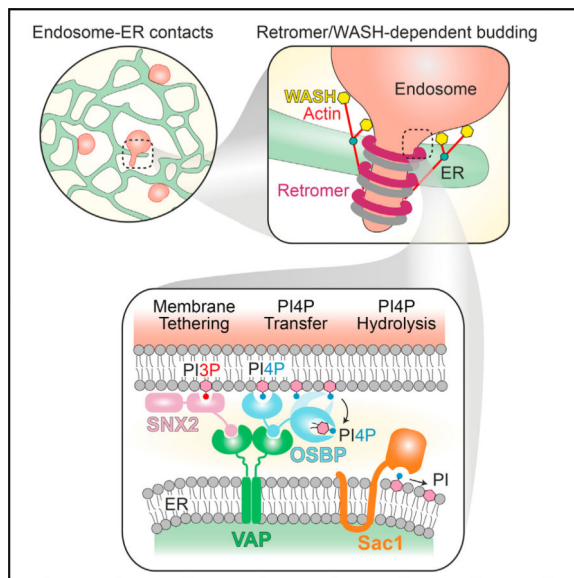*Correspondence: pietro.decamilli@yale.edu.
[7]Present address: Lee Kong Chian School of Medicine, Nanyang Technological University, Singapore 308232, Singapore

INTRODUCTION

Trafficking of bilayer lipids within cells occurs both via vesicular transport and via lipid transfer proteins that directly carry them through the aqueous environment of the cytosol. At least a fraction of this direct transport occurs at contacts between membranes not leading to membrane fusion (Giordano et al., 2013; Holthuis and Menon, 2014; Lahiri et al., 2015; Levine and Loewen, 2006; Manford et al., 2012; Saheki et al., 2016; Stefan et al., 2011). Major players in direct lipid transport between the endoplasmic reticulum (ER) and other membranes are VAPA and VAPB (Scs2 and Scs22 in yeast), two homologous tail-anchored ER membrane proteins (Levine and Loewen, 2006). VAPs comprise an N-terminal MSP domain, which binds a variety of lipid transfer proteins containing the so-called FFAT motif (two phenylalanine in an acidic tract), a coiled-coil region responsible for homo/ heterodimerization, and a C-terminal membrane anchor (Kaiser et al., 2005; Murphy and Levine, 2016). Several lipid transfer proteins that bind VAP through a FFAT motif can also bind other membranes in *trans*, thus tethering the ER to other membranes, while the lipid transfer module mediates lipid exchange (de Saint-Jean et al., 2011; Mesmin et al., 2013; Stefan et al., 2011).

Mutations in the MSP domain of VAPB (also called ALS8) that disrupt FFAT motif binding are responsible for a dominant form of amyotrophic lateral sclerosis (ALS) (Nishimura et al., 2004). It remains unclear whether the disease results from a dominant-negative effect of the mutant protein or from haploinsufficiency (Kabashi et al., 2013; Papiani et al., 2012; Teuling et al., 2007). Elucidating the impact of VAP loss-of-function may thus illuminate mechanisms of disease in addition to providing insights into fundamental aspects of lipid dynamics.

A major class of VAP interactors are members of the OSBP/ORP family (Osh proteins in yeast), which are defined by the presence of a lipid harboring module, the so-called OSBP-related domain (ORD). These proteins were originally thought to be dedicated to sterol

transport (Dawson et al., 1989; Im et al., 2005; Olkkonen and Levine, 2004). However, recent studies suggested that they have heterogeneous lipid transport or countertransport functions, with a major shared property being the transport of PI4P (Chung et al., 2015; de Saint-Jean et al., 2011; Maeda et al., 2013; Mesmin et al., 2013; Moser von Filseck et al., 2015). Several ORPs also have a PI4P-binding PH domain (Hammond and Balla, 2015). Via such domain, ER-anchored ORPs bind adjacent PI4P containing membranes, thus making available PI4P to the ER localized PI 4-phosphatase Sac1. Yeast cells that lack VAP (Scs2;Scs22 double mutants) have greatly elevated levels of plasma membrane PI4P (Stefan et al., 2011).

To gain further insight into the function(s) of VAP in cell physiology, we have studied the effects of the combined absence of VAPA and VAPB in human cells, with an emphasis on the impact of this perturbation on PI4P dynamics. VAP double knockout (KO) cells have major perturbations in PI4P levels and localization with a surprising very robust accumulation of PI4P on endosomes due to the impaired function of OSBP (and possibly of other ORPs). These changes lead to a disruption of the endosome-Golgi complex boundary that results, at least in part, by dysfunction of the retromer and the WASH complex.

RESULTS

TALEN-Mediated Knockout of Human VAPs

A TALEN-based gene-editing approach (Sanjana et al., 2012) was used to abolish VAP expression in HeLa cells. TALEN pairs specific to exon 2 of VAPA and VAPB, which encodes a stretch of amino acids highly conserved within the MSP domain, were chosen (Figure 1A). This stretch includes the proline whose mutation in VAPB is responsible for ALS8 and abolishes FFAT motif binding (Kim et al., 2010). After validation of gene targeting, three independent VAP double KO cell clones (DKO-1, DKO-2, and DKO-3) were selected where loss of VAPA (a doublet of two splice variants in wild-type cells), and VAPB was confirmed by western blotting (Figure 1B). Importantly, all three clones (referred to henceforth as VAP DKO cells) behaved similarly with regards to the phenotypic defects discussed in this paper.

Increased Abundance of PI4P on Endosomes in VAP DKO Cells

Levels of PI4P relative to total phosphoinositides, as detected by metabolic labeling with [^{3}H]inositol followed by HPLC analysis, were ~40% higher than in wild-type (WT) cells (Figure 1C). No obvious intensity change was observed in the labeling of the plasma membrane by probes that recognize PI4P in this membrane: N-PH$_{ORP5}$-GFP and GFP-2xPH$_{OSH2}$ (Figures 1D and 1E) (Chung et al., 2015; Hammond and Balla, 2015). In contrast, increased fluorescence in VAP DKO cells was observed with probes that recognize intracellular PI4P pools: GFP-P4C$_{SidC}$ and GFP-PH$_{OSBP}$ (Figures 1F and 1G) (Hammond and Balla 2015; Luo et al., 2015). These probes labeled the Golgi complex and, weakly, sparse vesicles throughout the cytoplasm in control cells. In VAP DKO cells, labeling of intracellular vesicles was strikingly stronger, and this difference was abolished by expression of VAPA or VAPB (Figure S1D). PI4P-positive vesicles were also positive for the endosomal markers Rab5 and Rab7 (Figure 1H).

A robust accumulation of PI4P on intracellular vesicles in DKO cells was confirmed by the observation that these vesicles were sites of ectopic $PI(4,5)P_2$ production by type I PIP kinases (Doughman et al., 2003), i.e., the lipid kinases that use PI4P as a substrate. $PI(4,5)P_2$, as revealed by the iRFP-PH$_{PLC\delta1}$ probe, is typically selectively concentrated at the plasma membrane (Hammond and Balla, 2015). This was the case in both untreated control and VAP DKO cells. Upon acute phospholipase C (PLC) activation, as achieved by addition of the muscarinic receptor agonist Oxo-M to cells transiently transfected with the muscarinic acetylcholine receptor (M1R) (Willars et al., 1998), $PI(4,5)P_2$ was massively hydrolyzed, leading to a redistribution of the $PI(4,5)P_2$ probe to the cytosol (Figures 1J and S1F). Such $PI(4,5)P_2$ loss rapidly triggered, as expected, a compensatory burst of $PI(4,5)P_2$ synthesis from PI4P, further accelerated by the addition of the muscarinic receptor antagonist atropine. As assessed by total internal reflection fluorescence (TIRF) microscopy, dissociation and reassociation of iRFP-PH$_{PLC\delta1}$ from and with the plasma membrane had similar kinetics in WT and VAP DKO cells (Figures S1F and S1G). Strikingly, however, while $PI(4,5)P_2$ resynthesis occurred nearly selectively at the plasma membrane in WT cells, it occurred first on internal vesicles and in the Golgi complex in VAP DKO cells (Figures 1J and 1K; Movie S1), consistent with the ectopic abundance of PI4P on such structures. Concomitant analysis of PI4P (GFP-PH$_{OSBP}$) and $PI(4,5)P_2$ (iRFP-PH$_{PLC\delta1}$) during the recovery from Oxo-M stimulation demonstrated direct conversion of PI4P to $PI(4,5)P_2$ on the internal membranes (Figures 1L and 1M) where ectopic presence of a PI4P 5-kinase (PIPKIg-87kD) was also detected (Di Paolo et al., 2002) (Figures 1N and 1O). Collectively, these observations demonstrated a strong elevation of PI4P on endosomes in VAP DKO cells.

Loss of OSBP and Sac1 Also Results in Increased PI4P Abundance on Endosomes

Recent studies have suggested a model according to which OSBP/ORP family proteins cooperate with the ER-localized PI 4-phosphatase Sac1 to negatively regulate PI4P on subcellular membranes (Chung et al., 2015; Mesmin et al., 2013; Moser von Filseck et al., 2015; Stefan et al., 2011). So far, OSBP has been reported to associate primarily with Golgi membranes (Mesmin et al., 2013). However, not only the PH domain-only of OSBP (a PI4P probe) (Figure 1G), but endogenous OSBP itself displayed a robust accumulation on endosomes in VAP DKO cells and such accumulation was rescued by expression of VAP (Figure 2A). OSBP is a FFAT motif containing VAP interactor. Thus, in the absence of VAP, the accumulation of PI4P on endosomes may at least in part reflect the impaired ability of OSBP delivering PI4P to Sac1 for degradation. Supporting this hypothesis, RNAi-mediated knockdown (KD) of OSBP resulted in a major increase of PI4P on endosomes as revealed by the PI4P probes GFP-PH$_{OSBP}$ and GFP-P4C$_{SidC}$ (Figures 2B–2E). Note that OSBP KD did not produce an obvious change in PI4P abundance at the plasma membrane, as assessed by GFP-P4C$_{SidC}$ and also by N-PH$_{ORP8L}$, a low-affinity PI4P probe that labels selectively the plasma membrane pool of PI4P (Figures 2F and 2G) (Chung et al., 2015). This was not unexpected, as key players in the regulation of plasma membrane PI4P are ORP5 and ORP8, two ORPs that are anchored at the ER independently of VAP (Chung et al., 2015).

Importantly, knockout (KO) of Sac1 by CRISPR/Cas9 (Figures 2H and S2A; Supplemental Experimental Procedures) resulted in a very robust increase in GFP-P4C$_{SidC}$ signal both at

the plasma membrane and on intracellular membranes (Figure 2K), indicating a functional partnership of Sac1 with both OSBP and ORP5/ORP8. This was confirmed by the expression in control and Sac1 KO cells of GFP-PH$_{OSBP}$ (Figure 2J) and N-PH$_{ORP8L}$ GFP (Figures 2L and 2M), which recognize PI4P selectively on internal membranes and in the plasma membrane (Chung et al., 2015), respectively. The collective signal generated by these probes was elevated in Sac1 KO cells (Figure S2B).

We conclude that VAP plays a critical role in the downregulation of PI4P on endosomes at least in part by making accessible PI4P to ER localized phosphatase Sac1.

Loss of VAP Disrupts Traffic between Endosomes and the Golgi Complex

While the occurrence of pleotropic defect can be expected in VAP DKO cells, given the multiple interactors of VAP (Murphy and Levine, 2016), the abnormal abundance of PI4P on endosomes prompted us to focus on defects in these compartments. A profound disruption of traffic at the endosome-Golgi interface was observed. As revealed by immunofluorescence, TGN46, a TGN protein in WT cells, was partially scattered throughout the cytoplasm of DKO cells as small puncta that colocalized with endosomal markers, such as EEA1 and the retromer subunit Vps35 (Bonifacino and Rojas, 2006; Hierro et al., 2007; Seaman et al., 1998) (Figures 3A–3C). Likewise, in DKO cells, marker proteins of the *trans*-Golgi, ST-mRFP, and GalT-EGFP (mRFP and EGFP fusions of sialyltransferase and galactosyltransferase fragments, respectively) (Cole et al., 1996; Schaub et al., 2006), were observed on puncta that colocalized with Rab5, Rab7, and the retromer component VPS29 (Figures 3D–3F). A similar scattered distribution was observed previously for endogenous galactosyltransferase in VAPA and VAPB double knock down cells (Peretti et al., 2008). No change was observed in the localization of several other Golgi complex proteins tested, such as GOLPH3 (Figure 3G), GRASP55 (Figure 3A), Golgin97, GM130, GRASP65, and P230 (Figures S3A and S3B), indicating that absence of VAP does not affect the Golgi complex globally.

Endosomes and the Golgi complex are continuously interconnected by bidirectional traffic. The accumulation of proteins of distal Golgi compartments in endosomes of VAP DKO cells suggested that VAP is required for proper transport between these two compartments. One such mechanism involves the retromer, a coat that controls exit from endosomes of Golgi-bound proteins by generating tubular buds and selecting their cargo, such as the cation-independent mannose-6-phosphate receptor (CI-MPR) (Bonifacino and Rojas, 2006; Burd and Cullen, 2014; Seaman et al., 1998). This receptor shuttles between the Golgi complex and endosomes and is also present at low levels at the plasma membrane. In WT cells, CI-MPR is primarily enriched in the Golgi complex in a retromer-dependent way (Bonifacino and Rojas, 2006). Accordingly, following 1 hr incubation of WT cells in the presence of an antibody that recognizes the extra cytosolic portion of CI-MPR exposed at the cell surface, the internalized antibody had primarily accumulated in the Golgi complex. In contrast, the antibody had accumulated only in peripheral endosomal vesicles in DKO cells, consistent with retromer dysfunction (Figure 3H), and this defect was rescued by re-expression of either VAP (Figures S3C and S3D).

A Physical Link between the Retromer and VAP

The ER makes contacts with endosomes, including VAP-dependent contacts (Alpy et al., 2013; Raiborg et al., 2015; Rocha et al., 2009). As some of the ER-endosome contacts occur at retromer-dependent budding sites (Rowland et al., 2014), we hypothesized that the retromer itself may interact with VAP. Inspection of a high-throughput VAP interactome (Huttlin et al., 2015) revealed as one of the top hits SNX2, a component of the membrane deformation subcomplex of the retromer (Bonifacino and Rojas, 2006). The potential significance of this finding was assessed by transfection experiments (and thus overexpression) in COS-7 cells, which are optimally suited for the imaging of ER architecture.

When expressed independently, YFP-SNX2 had the punctate localization that reflects its PI3P-dependent (via its PX domain) localization on endosomes (Burd and Cullen, 2014), while mCh-VAPA and mCh-VAPB had a diffuse distribution throughout the ER as expected. When YFP-SNX2 was co-expressed with either mCh-VAPA or mCh-VAPB, focal accumulation of VAP was observed at SNX2-positive endosomes (Figures 4A, 4D, and S4A). Such accumulation did not occur upon expression of other retromer proteins, such as SNX5, SNX6, or even of SNX1, the paralogue of SNX2 (Figures S4C, S4D, and 4C, respectively). Furthermore, acute depletion of endosomal PI3P by pharmacological inhibition of the type III PI 3-kinase VPS34 with VPS34-IN1 (Bago et al., 2014), not only resulted in the dissociation of SNX2 from endosomes to the cytosol (Burd and Cullen, 2014), as expected, but also in the dispersion of VAP, which re-acquired its uniform distribution throughout the ER (Figure 4B; Movie S2).

Further experiments demonstrated a direct interaction between SNX2 and VAP. First, SNX2 and VAPB were coprecipitated from detergent solubilized cell extracts (Figure 4E). In contrast, neither coprecipitation, as assessed by western blotting (Figure 4E) or mass spectrometry (Figures S4E and S4F) of the immunoprecipitates, nor coclustering, as assessed by microscopy (Figure 4F), was observed when WT VAPB was replaced by an FFAT motif-binding-deficient VAPB mutant (double K87D and M89D mutations, referred to as VAPB^{KMDD}) (Kaiser et al., 2005). The ALS-associated P56S mutation of VAPB, known to result in the misfolding of its FFAT-binding domain (the MSP domain), also inhibited coclustering (Figure 4G). Second, coclustering of SNX2 and VAPB required the N-terminal region of SNX2 (Figures 4I and S4B), which contains amino acid stretches reported to fit an FFAT-like consensus (Murphy and Levine, 2016) (Figure 4H). Mutation of phenylalanines in these motifs abolished (F28) or strongly reduced (F74) the interaction, as assessed by coprecipitation and coclustering (Figures 4H and 4J).

These findings reveal a direct functional link between VAP and retromer. As VAP occurs as a dimer that can further oligomerize (Kaiser et al., 2005; Kim et al., 2010), the binding of VAP to SNX2 may help bring OSBP in proximity of the retromer. Accordingly, we observed that cotransfected OSBP-EGFP, iRFP-SNX2, and mCherry-VAPB colocalized at the same hotspots (Figure 4K).

Accumulation of Actin on Endosomes Leading to Actin Comets

Live-cell imaging showed that endosome-Golgi hybrid vesicles of DKO cells had very high mobility. As retromer budding is assisted by a transient local burst of actin (Puthenveedu et al., 2010), we examined actin organization in DKO cells. F-actin staining with fluorescent phalloidin revealed loss of stress fibers (the predominant form of actin in control HeLa cells, Figure 5A) and presence of numerous and prominent actin foci or elongated structures located deep in the cytoplasm (Figures 5B and S5B). These changes could be rescued by exogenously expressing WT VAPA or VAPB, but not VAPB^{KMDD} or by expression of the MSP domain of VAPB alone, which is not anchored to the ER (Figures S5D–S5G). No major changes were observed in the microtubule cytoskeleton (Figure S5A).

The actin phenotype revealed by phalloidin was confirmed by observations of live cells expressing the GFP- or mCherry-tagged calponin homology domain of utrophin (CH$_{Utrophin}$), an F-actin reporter that also allowed identification of these structures as actin comets (Ferguson et al., 2009). Actin comets, also called actin tails, are bundles of highly dynamic actin that push organelles within the cytoplasm as a result of actin polymerization at the organelle interface and actin depolymerization at the opposite end. Consistent with a high turnover rate of actin in these structures, they disappeared more rapidly than stress fibers upon treatment with latrunculin, which impairs actin polymerization (Figure S5C) (Puthenveedu et al., 2010). Comets tips were positive for endosomal Rabs (Rab5, Rab7), the *trans*-Golgi marker proteins TGN46-EGFP and GalT-EGFP, the retromer cargo M6PR, and retromer components (such as Vps29 and SNX2) (Figures 5C and 5F; Movie S3), thus indicating that the high motility of the endosome-Golgi hybrid vesicles is due to their property to nucleate actin.

Actin Comets of VAP DKO Cells Are Nucleated by WASH

Previously described actin comets propelling endogenous organelles are nucleated by N-WASP, a Wiskott-Aldrich syndrome family member. Such comets are typically observed under conditions where PI(4,5)P$_2$ ectopically accumulates on intracellular vesicles (Rozelle et al., 2000). Like N-WASP and PI(4,5)P$_2$-dependent actin tails, actin tails of VAP DKO cells were Arp2/3 positive (Figure 5E). However, they were generally more centrally localized in the cell (Figure 5B). Furthermore, their tips were negative for N-WASP and for endocytic proteins typically found at the tips of PI(4,5)P$_2$-dependent tails including clathrin coat-associated factors such as SNX9 (Nandez et al., 2014) (Figures S6A and S6B). This difference was directly demonstrated in VAP DKO cells upon overexpression of the PI4P 5-kinase PIP5K1γ87 (Di Paolo et al., 2002) to generate PI(4,5)P$_2$-dependent comets. In these cells, PIP5K1γ87 was only observed at the tip of a subset of actin tails, which were thick and long, clearly distinct from the shorter, thinner actin comets induced by loss of VAP (Figures S6C and S6D). This prompted us to explore the potential presence of WASH, another member of the Wiskott-Aldrich protein family, at the tips of tails in VAP DKO cells (Derivery et al., 2009; Gomez and Billadeau, 2009). WASH is part of a complex that interacts with the retromer via its FAM21 subunit and that assists the retromer-dependent budding reaction by nucleating actin at bud sites on endosomes (Harbour et al., 2012).

Immunofluorescence revealed the presence of both WASH and FAM21 at all comet tips in VAP DKO cells (Figures 6A and 6B). This was confirmed by live microscopy of DKO cells co-expressing YFP-FAM21 with CH$_{UTR}$-mCh (Figure 6C; Movie S4). Accordingly, KD of either WASH or FAM21 (FAM21 KD resulted in the concomitant loss of WASH) suppressed the actin tail phenotype in VAP DKO cells (Figures 6F–6I). Consistent with the hybrid endosome-Golgi nature of organelles at the tip of the tails, the endosomal marker EEA1 (Figure 6C) and the Golgi marker ST-mRFP (Figure 6E) were juxtaposed to WASH. Additionally, morphometric analysis of immunofluorescence images showed that pixel intensity for WASH immunoreactivity, but not for EEA1 immunoreactivity, increased in VAP DKO cells relative to WT cells (Figures 6C and 6D), revealing a greater pool of assembled WASH.

PI4P and WASH-Mediated Actin Nucleation

Actin nucleation by WASH at retromer-dependent budding sites on endosomes is tightly controlled in WT cells (Puthenveedu et al., 2010). Exaggerated actin nucleation in VAP DKO cells could result from an altered balance between "on" and "off" signals underlying such nucleation.

In the case of N-WASP-dependent actin comets, it is the balance between PI(4,5)P$_2$ synthesis and dephosphorylation that controls actin nucleation (Nandez et al., 2014; Rozelle et al., 2000). Thus, we considered a role of endosomal phosphoinositides in the enhanced nucleation of WASH-dependent actin resulting from the lack of VAP. We ruled out PI3P, as inhibition of its synthesis on endosomes via the VPS34 inhibitor VPS34-IN1 (Bago et al., 2014) did not inhibit actin nucleation and in fact it stimulated it: it enhanced WASH recruitment both in WT and in VAP DKO cells, with the formation of actin comets in WT cells and exaggeration of actin on endosomes of DKO cells (Figure 6J). In some cells, where the inhibitor resulted in dramatically enlarged endosomes, actin tails were particularly prominent (Figure 6K; Movie S5).

To assess a potential role of abnormally elevated PI4P, we examined whether enhanced WASH-dependent actin nucleation could be mimicked by the loss of OSBP, which, as shown above, also results in such elevation. In OSBP KD cells, where endosomes (EEA1) became more clustered (Figure S7G), a robust enhancement of WASH immunoreactivity was detected on these organelles, along with the presence of assembled actin (Figures 7A and 7B), which at close inspection was represented by actin tails (Figures 7C and 7D; Movie S6). The presence not only of WASH, but also of FAM21, the *trans*-Golgi marker protein GalT-EGFP, Rab5, and Rab7 at the tips of the tails confirmed their similarity to the tails observed in VAP DKO cells (Figures 7C and 7D). Importantly, the additional KD of WASH in OSBP KD cells abolished the internal actin foci (Figure 7E). Further supporting a role of a complex involving OSBP, VAP and the retromer in the negative regulation of PI4P on endosomes, the KD of SNX2 also resulted in an increase of intracellular actin very similar to that produced by the KD of OSBP (Figures 7F–7J).

WASH-Mediated Actin Nucleation Is Impaired by the Knockdown of Type II PI 4-Kinases

If endosomal PI4P is required for the formation of actin tails in VAP DKO cells, impairment of PI4P synthesis should impair their formation. Mammalian genome encodes four PI 4-

kinases. Neither inhibition of PI4KIIIα, which acts primarily at the plasma membrane (Nakatsu et al., 2012) (with the A1 compound) (Bojjireddy et al., 2014), nor inhibition of PI4KIIIβ, which acts primarily in the Golgi complex (Godi et al., 1999) (with the PIK-93 compound) (Knight et al., 2006), had a major impact on actin comets and on the presence of PI4P on the endosome-*trans*-Golgi vesicles, although they reduced PI4P levels at the plasma membrane and the Golgi complex respectively, as expected (Figures S7A–S7D). No specific inhibitors are available for the two type II PI 4-kinases PI4KIIα and PI4KIIβ, which have a predominant endosomal localization (Balla et al., 2002) and thus could be the key players in PI4P generation on the hybrid endosome-*trans*-Golgi organelles. Importantly, GFP fusions of these two kinases and PI4P probe were detected at the tips of actin comets in DKO cells, supporting this possibility (Figure 7K; Movie S7). Strong reduction of the endogenous levels of these two kinases by small interfering RNA (siRNA)-dependent KD, as validated by western blotting (Figure 7O), drastically decreased the PI4P probe signal (GFP-P4C$_{SidC}$ and GFP-PH$_{OSBP}$) on hybrid endosome-Golgi vesicles (Figures 7N and 7P). Correspondingly, the KD of the two PI4KIIs decreased the abundance of phalloidin-detectable actin foci in VAP DKO cells and restored abundance of stress fibers (Figures 7L and 7M, top fields). It also reversed the intense enrichment of WASH immunoreactivity on EEA1-positive endosomes (Figures 7L and 7M, bottom fields). These results strongly support a role of PI4P in WASH-dependent actin nucleation and show that PI4KIIα and PI4KIIβ are the enzymes responsible for the generation of this PI4P pool.

DISCUSSION

We have shown that VAP-dependent ER-endosome contacts involving the retromer subunit SNX2 and OSBP have an impact on PI4P dynamics on endosomes. Via this action, VAP affects the interrelated functions of the retromer and WASH on these organelles, providing a new example of cross-talk between organ-elles mediated by direct contacts not leading to fusion.

The robust increase of PI4P in response to the lack of VAP is consistent with growing evidence that VAP helps, primarily via OSBP/ORP proteins, to generate bridges between the ER and other membranes that make accessible PI4P to the ER localized PI4P phosphatase Sac1. This may occur via delivery of PI4P to the ER by the transport activity of these proteins (Chung et al., 2015; Mesmin et al., 2013; Moser von Filseck et al., 2015) or, as proposed by others, by in *trans* action of Sac1 on the adjacent membrane (Dickson et al., 2016; Stefan et al., 2011). In yeast, deletion of the two VAP homologs (Scs2 and Scs22) results in strong PI4P elevations, with the bulk of excessive PI4P being localized at the plasma membrane (Stefan et al., 2011). Loss of VAP results in increased PI4P levels also in mammalian cells. However, PI4P increase does not occur at the plasma membrane, possibly because two ORP proteins that do not require VAP for ER anchoring, ORP5 and ORP8, function in the negative regulation of PI4P at the ER-plasma membrane interface (Chung et al., 2015). Our results show in VAP DKO cells the major increase of PI4P occurs on intracellular membranes (endosomes) and implicates impaired recruitment of OSBP in this change. OSBP was shown to control PI4P at the Golgi complex (Mesmin et al., 2013), but our study suggests its additional role at endosomes. PI4P elevation on endosomes in VAP DKO cells cannot be explained by a spillover of PI4P from the Golgi complex, as it is not

rescued by the pharmacological inhibition of PI4KIIIβ, the major player in the synthesis of PI4P in the Golgi complex. It is abolished, however, by the KD of PI4KIIα and PI4KIIβ, the two PI4Ks with an endosomal site of action (Burgess et al., 2012; Henmi et al., 2016; Minogue et al., 2006; Ryder et al., 2013). Other ORPs likely cooperate with OSBP in the actions reported here (Olkkonen and Levine, 2004), but the effects produced by the KD of OSBP strongly indicate its major involvement.

The increase of PI4P on endosomes observed in VAP DKO cells was accompanied by an accumulation of proteins of the *trans*-Golgi on endosomes, suggesting that the efficiency of sorting mechanisms that control traffic between the two organelles is compromised. This was consistent with the link that we have found between VAP and the retromer subunit SNX2. The function of retromer in fission of membrane tubules from endosomes is tightly coupled to actin nucleated by WASH (Derivery et al., 2009; Gomez and Billadeau, 2009; Puthenveedu et al., 2010). It was therefore of interest that a most striking phenotype of DKO cells was a robust reorganization of actin, with the loss of stress fibers and the abundant presence of actin comets, which were nucleated by WASH on the hybrid endosome-*trans*-Golgi vesicles. The occurrence of actin comets indicates a persistent nucleation of actin with a loss of the mechanism(s) that normally terminate(s) this process. Downregulation of PI4P and fission of retromer-dependent tubules could be the events leading to termination of actin assembly in WT cells.

An exaggerated actin nucleation is reminiscent of what has been observed upon inhibition of fission at endocytic sites, where actin nucleation is promoted by N-WASP in a $PI(4,5)P_2$-dependent way (Merrifield and Kaksonen, 2014; Ferguson et al., 2009; Messa et al., 2014). PI4P may have an equivalent role in actin nucleation promoted by WASH. KD of type II PI 4-kinases in VAP DKO cells impaired the association of WASH with endosomes and actin comet formation. Conversely, KD of OSBP in WT cells resulted in the elevation of PI4P on intracellular vesicles and in WASH-dependent actin comets formation. Further supporting a role of PI4P in WASH dynamics, the WASH complex was reported to interact with type II PI 4-kinase (Ryder et al., 2013), and a genetic interaction was observed between the single *Drosophila* type II PI 4-kinase and the retromer (Burgess et al., 2012). Additionally, KD of PI4KIIα in mammalian cells impairs endosome traffic (Minogue et al., 2006). Surprisingly, inhibition of PI3P synthesis on endosomes enhanced WASH recruitment and actin nucleation. Possibly, PI4P is confined to endosomal microdomains in WT cells, and loss of PI3P disrupts this segregation allowing the PI4P domain to expand. As PI3P is required for retromer assembly at the endosomal surface, we suggest a hand-over mechanism from PI3P- to PI4P-dependent interactions in retromer/WASH-dependent budding. The robust WASH-dependent actin nucleation on endosomes upon loss of PI3P clearly indicates that WASH can function in actin nucleation independently of the retromer.

Recently, Rowland et al. (2014) showed that a large fraction of retromer-dependent tubular buds on endosomes undergo fission at sites where they are closely apposed to the ER and that are marked by the presence of FAM21, the linker between the retromer and WASH. VAP may be a component of ER-endosomes tethers at these sites and may impact the fission reaction via the recruitment of OSBP and PI4P downregulation. Focal accumulation of VAP at retromer positive sites can be detected only if SNX2 is overexpressed. However, in WT

cells a transient interaction of ER with endosomes involving endogenous retromer and endogenous VAP may have a physiological effect without resulting in a major accumulation of VAP.

In conclusion, the new insight into VAP function provided by this study advances our knowledge of mechanisms that control PI4P dynamics and membrane traffic at the endosome-Golgi complex interface and the role of PI4P in this regulation. This insight may be useful to understand mechanisms through which VAP mutations lead to disease. Mutations in subunits of the WASH complex (strumpellin) and of the retromer (VPS35), i.e., two complexes which, as our results show, have interrelated functions downstream of VAP, have been implicated in neurode-generative diseases, including Alzheimer's and Parkinson's (Small and Petsko, 2015; Valdmanis et al., 2007). Most interestingly, the VPS35 Parkinson mutation impairs its binding to WASH (Zavodszky et al., 2014). Further elucidation of the proteins network discussed here may help shed new light on pathogenetic mechanisms in these diseases.

EXPERIMENTAL PROCEDURES

An overview of experimental procedures is provided below. See the Supplemental Experimental Procedures for details.

Generation of VAP Knockout Cells with TALENs

Editing of gene targeting (disruption of exon 2) was validated by the Surveyor Nuclease assay. Gene-edited cells were enriched by fluorescence-based cell sorting using the surrogate reporter as published (Kim et al., 2011). Individual clones were isolated by limiting dilution and verification of targeted gene disruption was performed by PCR genotyping and sequencing.

Fluorescence Microscopy

For immunofluorescence, cells were grown on glass coverslips (Neuvitro), fixed with 4% paraformaldehyde (PFA) and then processed by standard procedures. To monitor CI-MPR internalization, cells were incubated at 37°C in serum-free DMEM containing 10 μg/ml mouse anti-CI-MPR monoclonal antibody (mAb) for up to 60 min, quickly rinsed with PBS, and then immunostained for the internalized antibodies. Imaging was performed by spinning disc confocal (SDC) microscopy, unless otherwise specified.

For live cell imaging, cells were plated on 35-mm glass bottom dishes (MatTek Corp) at low density, allowed to attach overnight, transfected, and imaged with a SDC microscope 16–20 hr after transfection. Spinning disc confocal (SDC) microscopy was performed as described in the Supplemental Experimental Procedures.

Phosphoinositide Analysis

WT and VAP DKO cells at similar confluency on 10-cm dishes were metabolically labeled with [^{3}H]myo-inositol (MP Biomedicals) in inositol-free DMEM (MP Biomedicals) for 48 hr. Subsequently, lipids were extracted, deacylated and [^{3}H]-labeled glycerophosphoinositol

moieties were separated using high performance liquid chromatography (Shimadzu Scientific Instruments) and detected by an online flow scintillation analyzer (B-RAM, IN/US).

Supplementary Material

Refer to Web version on PubMed Central for supplementary material.

ACKNOWLEDGMENTS

REFERENCES

Alpy F, Rousseau A, Schwab Y, Legueux F, Stoll I, Wendling C, Spiegelhalter C, Kessler P, Mathelin C, Rio M-C, et al. STARD3 or STARD3NL and VAP form a novel molecular tether between late endosomes and the ER. J. Cell Sci. 2013; 126:5500–5512. [PubMed: 24105263]

Bago R, Malik N, Munson MJ, Prescott AR, Davies P, Sommer E, Shpiro N, Ward R, Cross D, Ganley IG, Alessi DR. Characterization of VPS34-IN1, a selective inhibitor of Vps34, reveals that the phosphatidylinositol 3-phosphate-binding SGK3 protein kinase is a downstream target of class III phosphoinositide 3-kinase. Biochem. J. 2014; 463:413–427. [PubMed: 25177796]

Balla A, Tuymetova G, Barshishat M, Geiszt M, Balla T. Characterization of type II phosphatidylinositol 4-kinase isoforms reveals association of the enzymes with endosomal vesicular compartments. J. Biol. Chem. 2002; 277:20041–20050. [PubMed: 11923287]

Bojjireddy N, Botyanszki J, Hammond G, Creech D, Peterson R, Kemp DC, Snead M, Brown R, Morrison A, Wilson S, et al. Pharmacological and genetic targeting of the PI4KA enzyme reveals its important role in maintaining plasma membrane phosphatidylinositol 4-phosphate and phosphatidylinositol 4,5-bisphosphate levels. J. Biol. Chem. 2014; 289:6120–6132. [PubMed: 24415756]

Bonifacino JS, Rojas R. Retrograde transport from endosomes to the trans-Golgi network. Nat. Rev. Mol. Cell Biol. 2006; 7:568–579. [PubMed: 16936697]

Burd C, Cullen PJ. Retromer: a master conductor of endosome sorting. Cold Spring Harb. Perspect. Biol. 2014; 6:a016774. [PubMed: 24492709]

Burgess J, Del Bel LM, Ma C-IJ, Barylko B, Polevoy G, Rollins J, Albanesi JP, Krämer H, Brill JA. Type II phosphatidylinositol 4-kinase regulates trafficking of secretory granule proteins in Drosophila. Development. 2012; 139:3040–3050. [PubMed: 22791894]

Chung J, Torta F, Masai K, Lucast L, Czapla H, Tanner LB, Narayanaswamy P, Wenk MR, Nakatsu F, De Camilli P. Intracellular transport. PI4P/phosphatidylserine countertransport at ORP5- and ORP8-mediated ER-plasma membrane contacts. Science. 2015; 349:428–432. [PubMed: 26206935]

Cole NB, Smith CL, Sciaky N, Terasaki M, Edidin M, Lippincott-Schwartz J. Diffusional mobility of Golgi proteins in membranes of living cells. Science. 1996; 273:797–801. [PubMed: 8670420]

Dawson PA, Ridgway ND, Slaughter CA, Brown MS, Goldstein JL. cDNA cloning and expression of oxysterol-binding protein, an oligomer with a potential leucine zipper. J. Biol. Chem. 1989; 264:16798–16803. [PubMed: 2777807]

de Saint-Jean M, Delfosse V, Douguet D, Chicanne G, Payrastre B, Bourguet W, Antonny B, Drin G. Osh4p exchanges sterols for phosphatidylinositol 4-phosphate between lipid bilayers. J. Cell Biol. 2011; 195:965–978. [PubMed: 22162133]

Derivery E, Sousa C, Gautier JJ, Lombard B, Loew D, Gautreau A. The Arp2/3 activator WASH controls the fission of endosomes through a large multiprotein complex. Dev. Cell. 2009; 17:712–723. [PubMed: 19922875]

Di Paolo G, Pellegrini L, Letinic K, Cestra G, Zoncu R, Voronov S, Chang S, Guo J, Wenk MR, De Camilli P. Recruitment and regulation of phosphatidylinositol phosphate kinase type 1 gamma by the FERM domain of talin. Nature. 2002; 420:85–89. [PubMed: 12422219]

Dickson EJ, Jensen JB, Vivas O, Kruse M, Traynor-Kaplan AE, Hille B. Dynamic formation of ER-PM junctions presents a lipid phosphatase to regulate phosphoinositides. J. Cell Biol. 2016; 213:33–48. [PubMed: 27044890]

Doughman RL, Firestone AJ, Anderson RA. Phosphatidylinositol phosphate kinases put PI4,5P(2) in its place. J. Membr. Biol. 2003; 194:77–89. [PubMed: 14502432]

Ferguson SM, Raimondi A, Paradise S, Shen H, Mesaki K, Ferguson A, Destaing O, Ko G, Takasaki J, Cremona O, et al. Coordinated actions of actin and BAR proteins upstream of dynamin at endocytic clathrin-coated pits. Dev. Cell. 2009; 17:811–822. [PubMed: 20059951]

Giordano F, Saheki Y, Idevall-Hagren O, Colombo SF, Pirruccello M, Milosevic I, Gracheva EO, Bagriantsev SN, Borgese N, De Camilli P. PI(4,5)P$_2$-dependent and Ca(2+)-regulated ER-PM interactions mediated by the extended synaptotagmins. Cell. 2013; 153:1494–1509. [PubMed: 23791178]

Godi A, Pertile P, Meyers R, Marra P, Di Tullio G, Iurisci C, Luini A, Corda D, De Matteis MA. ARF mediates recruitment of PtdIns-4-OH kinase-beta and stimulates synthesis of PtdIns(4,5)P2 on the Golgi complex. Nat. Cell Biol. 1999; 1:280–287. [PubMed: 10559940]

Gomez TS, Billadeau DD. A FAM21-containing WASH complex regulates retromer-dependent sorting. Dev. Cell. 2009; 17:699–711. [PubMed: 19922874]

Hammond GRV, Balla T. Polyphosphoinositide binding domains: key to inositol lipid biology. Biochim. Biophys. Acta. 2015; 1851:746–758. [PubMed: 25732852]

Harbour ME, Breusegem SY, Seaman MNJ. Recruitment of the endosomal WASH complex is mediated by the extended 'tail' of Fam21 binding to the retromer protein Vps35. Biochem. J. 2012; 442:209–220. [PubMed: 22070227]

Henmi Y, Morikawa Y, Oe N, Ikeda N, Fujita A, Takei K, Minogue S, Tanabe K. PtdIns4KIIα generates endosomal PtdIns(4)P and is required for receptor sorting at early endosomes. Mol. Biol. Cell. 2016; 27:990–1001. [PubMed: 26823017]

Hierro A, Rojas AL, Rojas R, Murthy N, Effantin G, Kajava AV, Steven AC, Bonifacino JS, Hurley JH. Functional architecture of the retromer cargo-recognition complex. Nature. 2007; 449:1063–1067. [PubMed: 17891154]

Holthuis JCM, Menon AK. Lipid landscapes and pipelines in membrane homeostasis. Nature. 2014; 510:48–57. [PubMed: 24899304]

Huttlin EL, Ting L, Bruckner RJ, Gebreab F, Gygi MP, Szpyt J, Tam S, Zarraga G, Colby G, Baltier K, et al. The BioPlex Network: a systematic exploration of the human interactome. Cell. 2015; 162:425–440. [PubMed: 26186194]

Im YJ, Raychaudhuri S, Prinz WA, Hurley JH. Structural mechanism for sterol sensing and transport by OSBP-related proteins. Nature. 2005; 437:154–158. [PubMed: 16136145]

Kabashi E, El Oussini H, Bercier V, Gros-Louis F, Valdmanis PN, McDearmid J, Mejier IA, Dion PA, Dupre N, Hollinger D, et al. Investigating the contribution of VAPB/ALS8 loss of function in amyotrophic lateral sclerosis. Hum. Mol. Genet. 2013; 22:2350–2360. [PubMed: 23446633]

Kaiser SE, Brickner JH, Reilein AR, Fenn TD, Walter P, Brunger AT. Structural basis of FFAT motif-mediated ER targeting. Structure. 2005; 13:1035–1045. [PubMed: 16004875]

Kim S, Leal SS, Ben Halevy D, Gomes CM, Lev S. Structural requirements for VAP-B oligomerization and their implication in amyotrophic lateral sclerosis-associated VAP-B(P56S) neurotoxicity. J. Biol. Chem. 2010; 285:13839–13849. [PubMed: 20207736]

Kim H, Um E, Cho S-R, Jung C, Kim H, Kim J-S. Surrogate reporters for enrichment of cells with nuclease-induced mutations. Nat. Methods. 2011; 8:941–943. [PubMed: 21983922]

Knight ZA, Gonzalez B, Feldman ME, Zunder ER, Goldenberg DD, Williams O, Loewith R, Stokoe D, Balla A, Toth B, et al. A pharmacological map of the PI3-K family defines a role for p110alpha in insulin signaling. Cell. 2006; 125:733–747. [PubMed: 16647110]

Lahiri S, Toulmay A, Prinz WA. Membrane contact sites, gateways for lipid homeostasis. Curr. Opin. Cell Biol. 2015; 33:82–87. [PubMed: 25569848]

Levine T, Loewen C. Inter-organelle membrane contact sites: through a glass, darkly. Curr. Opin. Cell Biol. 2006; 18:371–378. [PubMed: 16806880]

Luo X, Wasilko DJ, Liu Y, Sun J, Wu X, Luo Z-Q, Mao Y. Structure of the Legionella virulence factor, SidC reveals a unique PI(4)P-specific binding domain essential for its targeting to the bacterial phagosome. PLoS Pathog. 2015; 11:e1004965. [PubMed: 26067986]

Maeda K, Anand K, Chiapparino A, Kumar A, Poletto M, Kaksonen M, Gavin A-C. Interactome map uncovers phosphatidylserine transport by oxysterol-binding proteins. Nature. 2013; 501:257–261. [PubMed: 23934110]

Manford AG, Stefan CJ, Yuan HL, Macgurn JA, Emr SD. ER-to-plasma membrane tethering proteins regulate cell signaling and ER morphology. Dev. Cell. 2012; 23:1129–1140. [PubMed: 23237950]

Merrifield CJ, Kaksonen M. Endocytic accessory factors and regulation of clathrin-mediated endocytosis. Cold Spring Harb. Perspect. Biol. 2014; 6:a016733. [PubMed: 25280766]

Mesmin B, Bigay J, Moser von Filseck J, Lacas-Gervais S, Drin G, Antonny B. A four-step cycle driven by PI(4)P hydrolysis directs sterol/ PI(4)P exchange by the ER-Golgi tether OSBP. Cell. 2013; 155:830–843. [PubMed: 24209621]

Messa M, Fernández-Busnadiego R, Sun EW, Chen H, Czapla H, Wrasman K, Wu Y, Ko G, Ross T, Wendland B, De Camilli P. Epsin deficiency impairs endocytosis by stalling the actin-dependent invagination of endocytic clathrin-coated pits. eLife. 2014; 3:e03311. [PubMed: 25122462]

Minogue S, Waugh MG, De Matteis MA, Stephens DJ, Berditchevski F, Hsuan JJ. Phosphatidylinositol 4-kinase is required for endosomal trafficking and degradation of the EGF receptor. J. Cell Sci. 2006; 119:571–581. [PubMed: 16443754]

Moser von Filseck J, opi A, Delfosse V, Vanni S, Jackson CL, Bourguet W, Drin G. Intracellular transport. Phosphatidylserine transport by ORP/Osh proteins is driven by phosphatidylinositol 4-phosphate. Science. 2015; 349:432–436. [PubMed: 26206936]

Murphy SE, Levine TP. VAP, a Versatile Access Point for the Endoplasmic Reticulum: Review and analysis of FFAT-like motifs in the VAPome. Biochim. Biophys. Acta 1861. 2016; (8 Pt B):952–961.

Nakatsu F, Baskin JM, Chung J, Tanner LB, Shui G, Lee SY, Pirruccello M, Hao M, Ingolia NT, Wenk MR, De Camilli P. PtdIns4P synthesis by PI4KIIIa at the plasma membrane and its impact on plasma membrane identity. J. Cell Biol. 2012; 199:1003–1016. [PubMed: 23229899]

Nandez R, Balkin DM, Messa M, Liang L, Paradise S, Czapla H, Hein MY, Duncan JS, Mann M, De Camilli P. A role of OCRL in clathrin-coated pit dynamics and uncoating revealed by studies of Lowe syndrome cells. Elife. 2014; 3:e02975. [PubMed: 25107275]

Nishimura AL, Mitne-Neto M, Silva HCA, Richieri-Costa A, Middleton S, Cascio D, Kok F, Oliveira JRM, Gillingwater T, Webb J, et al. A mutation in the vesicle-trafficking protein VAPB causes late-onset spinal muscular atrophy and amyotrophic lateral sclerosis. Am. J. Hum. Genet. 2004; 75:822–831. [PubMed: 15372378]

Olkkonen VM, Levine TP. Oxysterol binding proteins: in more than one place at one time? Biochem. Cell Biol. 2004; 82:87–98. [PubMed: 15052330]

Papiani G, Ruggiano A, Fossati M, Raimondi A, Bertoni G, Francolini M, Benfante R, Navone F, Borgese N. Restructured endoplasmic reticulum generated by mutant amyotrophic lateral sclerosis-linked VAPB is cleared by the proteasome. J. Cell Sci. 2012; 125:3601–3611. [PubMed: 22611258]

Peretti D, Dahan N, Shimoni E, Hirschberg K, Lev S. Coordinated lipid transfer between the endoplasmic reticulum and the Golgi complex requires the VAP proteins and is essential for Golgi-mediated transport. Mol. Biol. Cell. 2008; 19:3871–3884. [PubMed: 18614794]

Puthenveedu MA, Lauffer B, Temkin P, Vistein R, Carlton P, Thorn K, Taunton J, Weiner OD, Parton RG, von Zastrow M. Sequence-dependent sorting of recycling proteins by actin-stabilized endosomal microdomains. Cell. 2010; 143:761–773. [PubMed: 21111236]

Raiborg C, Wenzel EM, Pedersen NM, Olsvik H, Schink KO, Schultz SW, Vietri M, Nisi V, Bucci C, Brech A, et al. Repeated ER-endo-some contacts promote endosome translocation and neurite outgrowth. Nature. 2015; 520:234–238. [PubMed: 25855459]

Rocha N, Kuijl C, van der Kant R, Janssen L, Houben D, Janssen H, Zwart W, Neefjes J. Cholesterol sensor ORP1L contacts the ER protein VAP to control Rab7-RILP-p150 Glued and late endosome positioning. J. Cell Biol. 2009; 185:1209–1225. [PubMed: 19564404]

Rowland AA, Chitwood PJ, Phillips MJ, Voeltz GK. ER contact sites define the position and timing of endosome fission. Cell. 2014; 159:1027–1041. [PubMed: 25416943]

Rozelle AL, Machesky LM, Yamamoto M, Driessens MH, Insall RH, Roth MG, Luby-Phelps K, Marriott G, Hall A, Yin HL. Phosphatidylinositol 4,5-bisphosphate induces actin-based movement of raft-enriched vesicles through WASP-Arp2/3. Curr. Biol. 2000; 10:311–320. [PubMed: 10744973]

Ryder PV, Vistein R, Gokhale A, Seaman MN, Puthenveedu MA, Faundez V. The WASH complex, an endosomal Arp2/3 activator, interacts with the Hermansky-Pudlak syndrome complex BLOC-1 and its cargo phosphatidylinositol-4-kinase type IIa. Mol. Biol. Cell. 2013; 24:2269–2284. [PubMed: 23676666]

Saheki Y, Bian X, Schauder CM, Sawaki Y, Surma MA, Klose C, Pincet F, Reinisch KM, De Camilli P. Control of plasma membrane lipid homeostasis by the extended synaptotagmins. Nat. Cell Biol. 2016; 18:504–515. [PubMed: 27065097]

Sanjana NE, Cong L, Zhou Y, Cunniff MM, Feng G, Zhang F. A transcription activator-like effector toolbox for genome engineering. Nat. Protoc. 2012; 7:171–192. [PubMed: 22222791]

Schaub BE, Berger B, Berger EG, Rohrer J. Transition of galactosyltransferase 1 from trans-Golgi cisterna to the trans-Golgi network is signal mediated. Mol. Biol. Cell. 2006; 17:5153–5162. [PubMed: 17021253]

Seaman MN, McCaffery JM, Emr SD. A membrane coat complex essential for endosome-to-Golgi retrograde transport in yeast. J. Cell Biol. 1998; 142:665–681. [PubMed: 9700157]

Small SA, Petsko GA. Retromer in Alzheimer disease, Parkinson disease and other neurological disorders. Nat. Rev. Neurosci. 2015; 16:126–132. [PubMed: 25669742]

Stefan CJ, Manford AG, Baird D, Yamada-Hanff J, Mao Y, Emr SD. Osh proteins regulate phosphoinositide metabolism at ER-plasma membrane contact sites. Cell. 2011; 144:389–401. [PubMed: 21295699]

Teuling E, Ahmed S, Haasdijk E, Demmers J, Steinmetz MO, Akhmanova A, Jaarsma D, Hoogenraad CC. Motor neuron disease-associated mutant vesicle-associated membrane protein-associated protein (VAP) B recruits wild-type VAPs into endoplasmic reticulum-derived tubular aggregates. J. Neurosci. 2007; 27:9801–9815. [PubMed: 17804640]

Valdmanis PN, Meijer IA, Reynolds A, Lei A, MacLeod P, Schlesinger D, Zatz M, Reid E, Dion PA, Drapeau P, Rouleau GA. Mutations in the KIAA0196 gene at the SPG8 locus cause hereditary spastic paraplegia. Am. J. Hum. Genet. 2007; 80:152–161. [PubMed: 17160902]

Willars GB, Nahorski SR, Challiss RA. Differential regulation of muscarinic acetylcholine receptor-sensitive polyphosphoinositide pools and consequences for signaling in human neuroblastoma cells. J. Biol. Chem. 1998; 273:5037–5046. [PubMed: 9478953]

Zavodszky E, Seaman MNJ, Moreau K, Jimenez-Sanchez M, Breusegem SY, Harbour ME, Rubinsztein DC. Mutation in VPS35 associated with Parkinson's disease impairs WASH complex association and inhibits autophagy. Nat. Commun. 2014; 5:3828. [PubMed: 24819384]

Highlights

- An interaction between VAP and the retromer subunit SNX2 tethers the ER to endosomes

- Segregation of TGN proteins from endosomes is impaired in cells that lack VAP

- A PI4P pool regulated by OSBP accumulates on endosomes of VAP double KO cells

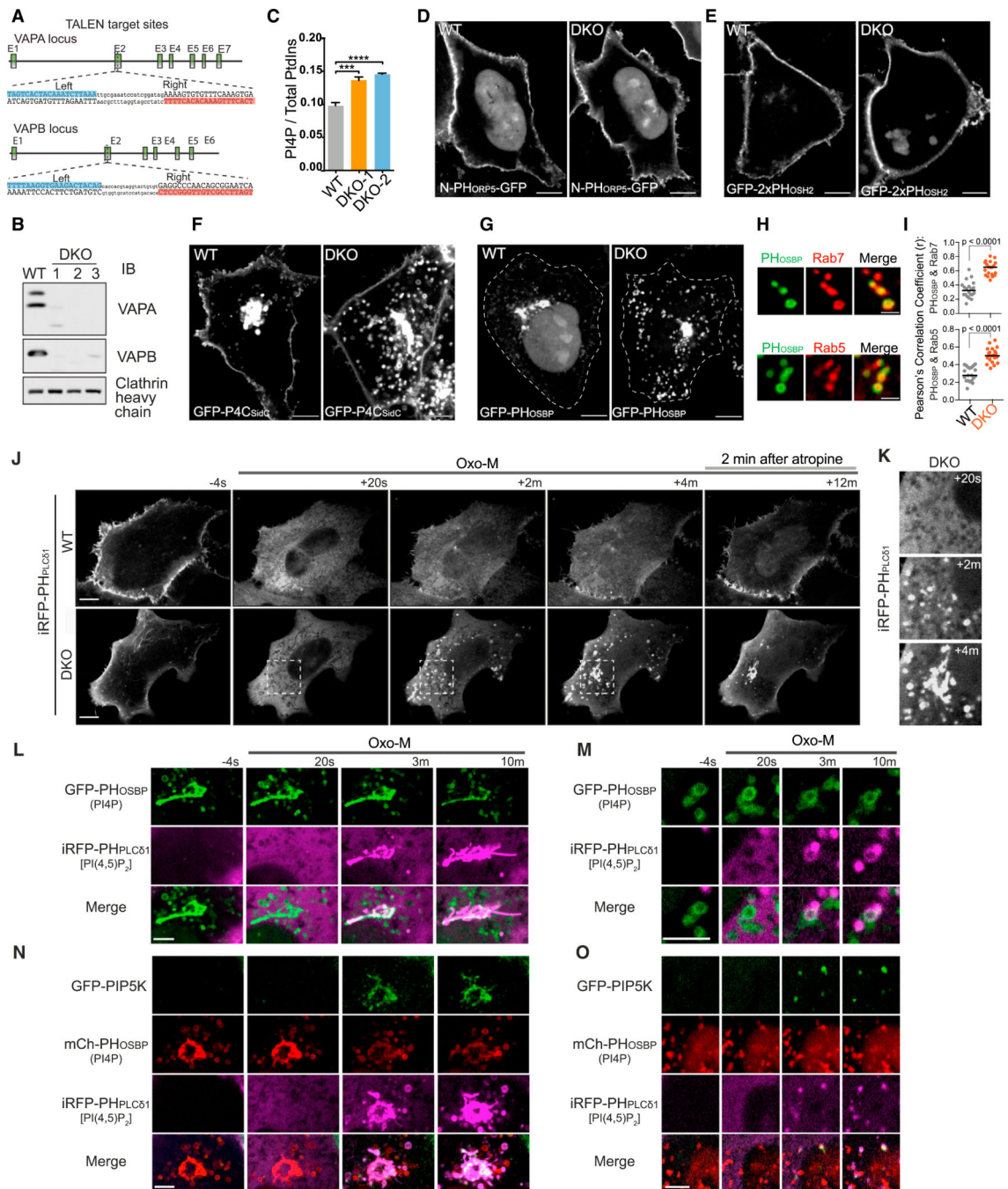- WASH mediates potent actin nucleation from endosomes in cells lacking VAP or OSBP

Figure 1. Increased Abundance of PI4P on Endosomes in VAP DKO Cells

(A) Schematic depiction of TALEN targeting sites in exon 2 of human VAPA and VAPB loci. The sequences targeted by the TALEN pairs are highlighted in blue (left arm) and red (right arm) respectively.

(B) Western blot of WT HeLa cells and of three independent VAP DKO HeLa cell lines.

(C) HPLC analysis of cell extracts showing an increased ratio of PI4P versus total inositol phospholipids in VAP DKO cells relative to WT cells. n = 3 independent experiments. Data

are represented as mean ± SEM. WT versus DKO-1, ***p = 0.007; WT versus DKO-2, ****p < 0.0001.

(D–G) Confocal images of WT and VAP DKO cells expressing four different PI4P probes: N-PH$_{ORP5}$-GFP (D) and GFP-2xPH$_{OSH2}$ (E), which label selectively PI4P at the plasma membrane, GFP-P4C$_{SidC}$ (F), which labels PI4P both at the plasma membrane and on internal membranes, and GFP-PH$_{OSBP}$ (G), which labels intracellular PI4P pools. Note the increase of PI4P on vesicular compartments, but no obvious PI4P accumulation at the plasma membrane in VAP DKO cells. Scale bar, 10 μm.

(H and I) Confocal images of VAP DKO cells co-expressing the PI4P probe GFP-PH$_{OSBP}$ and the endosome markers mCh-Rab7 and Rab5-mRFP, revealing the presence of PI4P on endosomes (H). Scale bar, 2 μm. Graph of Pearson's correlation coefficient shows greater colocalization of GFP-PH$_{OSBP}$ with mCh-Rab7 and Rab5-mRFP in VAP DKO cells (I) (n = 20 cells, two-tailed t test).

(J and K) Time-lapse confocal images of WT and VAP DKO cells co-transfected the PI(4,5)P$_2$ probe iRFP-PH$_{PLCd1}$ and the muscarinic receptor M1R. Oxo-M (20 μM) was added to cells at time 0 and the M1R antagonist atropine (50 μM) after 10 min. DKO cells show ectopic accumulation of PI(4,5)P$_2$ on intracellular vesicles. The region of the DKO cell indicated by a dashed box in (J) is shown at high magnification in (K). Scale bar, 10 μm. See also Movie S1.

(L–O) High-magnification time-lapse images of VAP DKO cells co-transfected with M1R and the indicated plasmids, showing the appearance of PI(4,5)P$_2$ in the PI4P-rich Golgi complex (L) and on a subset of PI4P-positive vesicles (M) in response to Oxo-M stimulation. PIP5K1γ87 also accumulates in the Golgi complex (N) and on a subset of intracellular vesicles (O) as they become PI(4,5)P$_2$ positive. Scale bar, 5 μm.
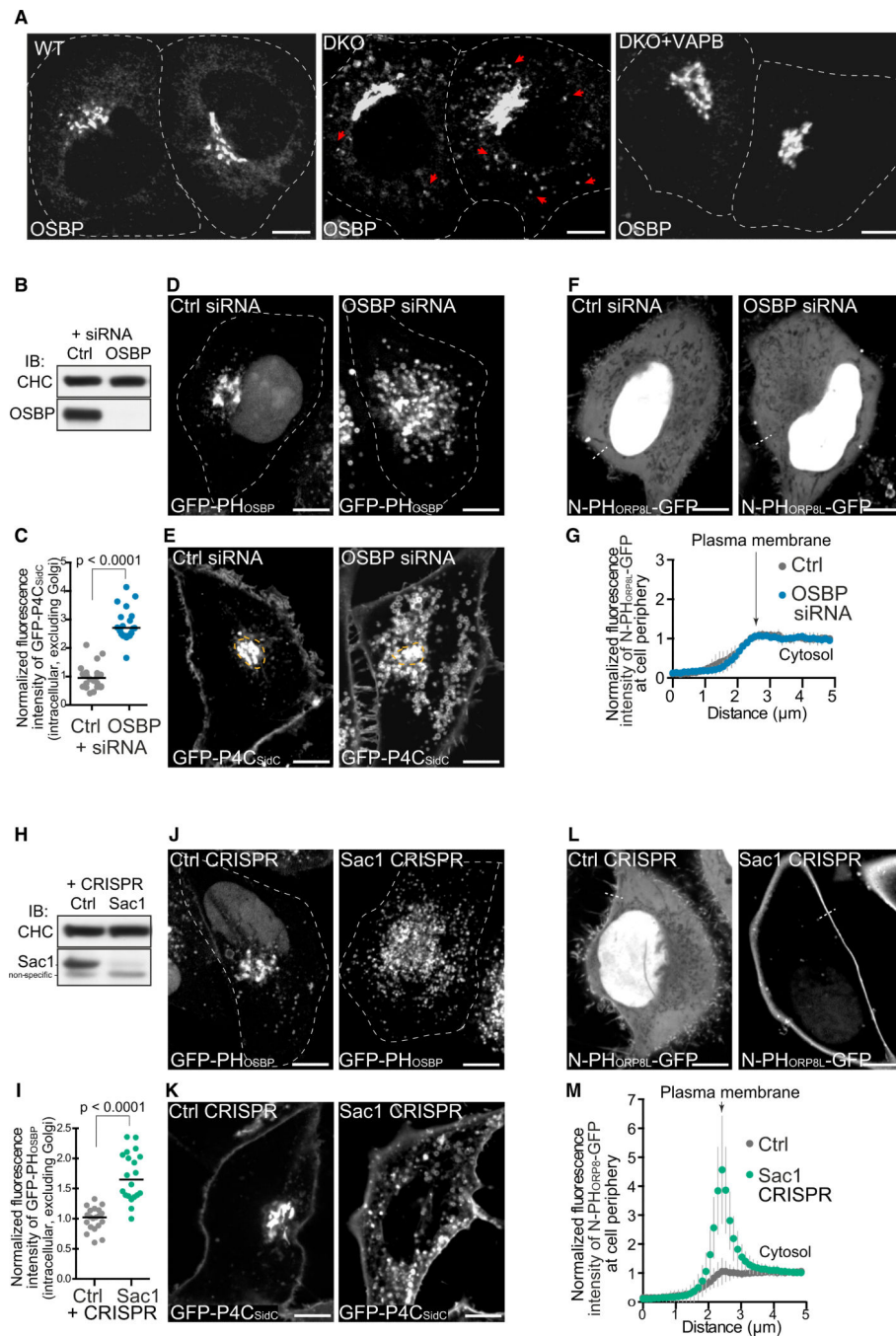
See also Figure S1.

Figure 2. Loss of OSBP and Sac1 Results in Increased PI4P Abundance on Endosomes

(A) Immunofluorescence revealing enhanced localization of endogenous OSBP on intracellular vesicles in VAP DKO cells (red arrowheads) and rescue of this change by exogenously expressed WT VAPB. Scale bar, 10 μm.

(B) Western blot of WT HeLa cells transfected with the indicated siRNAs showing depletion of OSBP protein in OSBP siRNA transfected cells.

(C–G) Confocal images of WT cells transfected with control or OSBP siRNA and expressing three distinct PI4P probes: GFP-PH$_{OSBP}$ (D), which label selectively internal

PI4P pools, GFP-P4C$_{SidC}$ (E), which label both internal and plasma membrane PI4P pools, and N-PH$_{ORP8L}$-GFP (F), a low-affinity "sensor" of plasma membrane PI4P that remains primarily in the cytosol/nucleus under control conditions. In OSBP siRNA-treated cells, GFP-P4C$_{SidC}$ (E) and GFP-PH$_{OSBP}$ (D) accumulate in vesicular compartments. No increase of PI4P in the plasma membrane is detected by any of these probes. Scale bar, 10 μm. (C and G) Quantifications of the vesicular fluorescence of GFP-PH$_{OSBP}$ and of the plasma membrane/cytosol N-PH$_{ORP8L}$-GFP fluorescence ratio based on line scans as exemplified in (F) (n = 20 cells for cells treated with control or OSBP siRNAs, two-tailed t test).

(H) Western blot of WT cells transfected with CRISPR/Cas9s constructs as indicated, showing the depletion of Sac1 protein in Sac1 CRISPR/Cas9 transfected cells.

(I–M) Confocal images of WT HeLa cells transfected with control or Sac1 CRISPR/Cas9 and expressing the same three distinct PI4P probes used for fields (D–F). In Sac1 CRISPR/Cas9-treated cells, GFP-PH$_{OSBP}$ (J) and GFP-P4C$_{SidC}$ (K) show a robust labeling of vesicles, and N-PH$_{ORP8L}$-GFP redistributes from the cytosol/nucleus to the plasma membrane (L), signaling a major increase of PI4P in all these membranes. Scale bar, 10 μm.

(I and M) Quantifications of the vesicular fluorescence of GFP-PH$_{OSBP}$ and of the plasma membrane/cytosol N-PH$_{ORP8L}$-GFP fluorescence ratio based on line scans (n = 20 cells for each genotype in I, two-tailed t test).
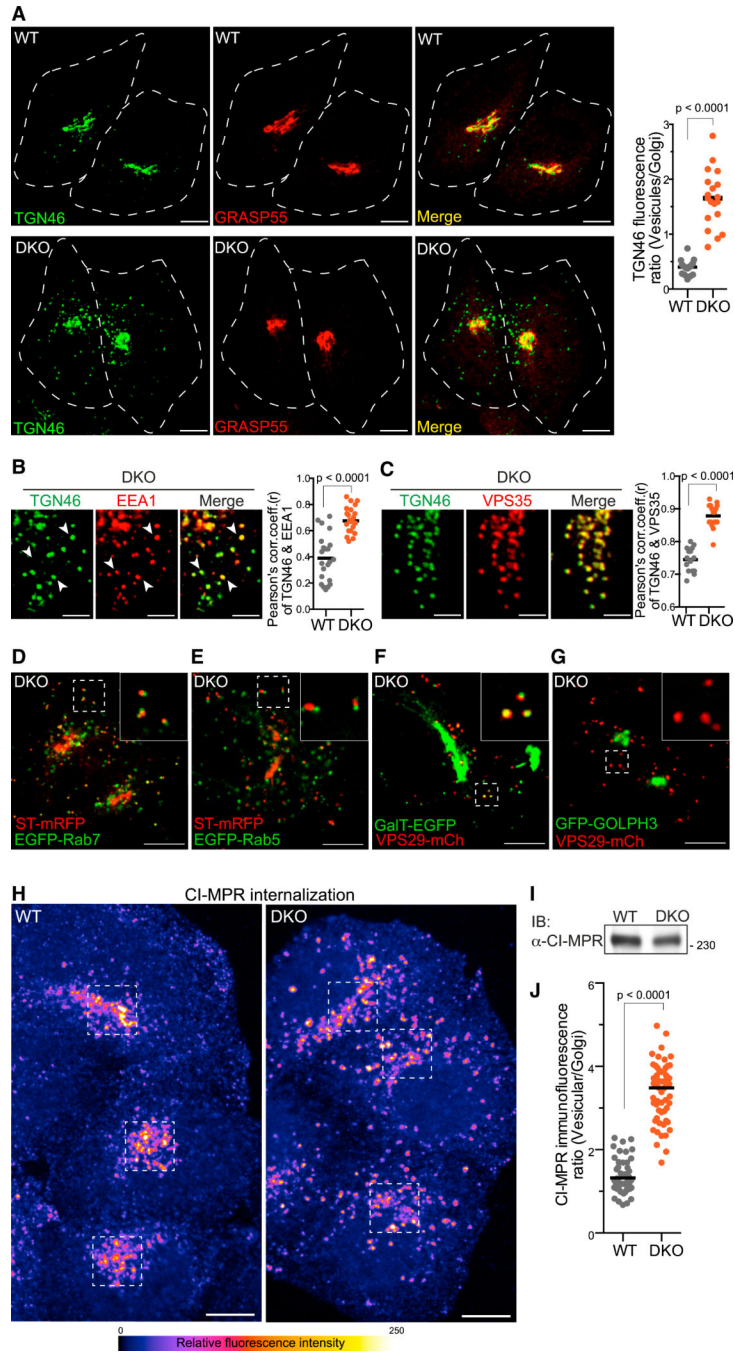
See also Figure S2.

Figure 3. Defects in Endosomes-to-Golgi Traffic in VAP DKO Cells

(A) TGN46 and GRASP55 immunofluorescence showing the Golgi localization of TGN46 in WT cells and its scattered distribution in the cytoplasm of VAP DKO cells. Scale bar, 10 μm. The graph at right shows the ratio of the punctate TGN46 fluorescence throughout the cytoplasm excluding the Golgi region, versus the TGN46 fluorescence within the Golgi region (n = 19 cells for each genotype, two-tailed t test).

(B and C) Close apposition of TGN46 and endosomal markers (EEA1 and VPS35) in DKO cells. Scale bar, 5 μm. Graphs of the Pearson's correlation coefficient shows greater

colocalization of TGN46 with EEA1 and VPS35 in VAP DKO cells than in WT (n = 22 cells for each genotype in B, n = 15 cells for WT and 17 cells for VAP DKO in C, two-tailed t test).

(D–E) Snapshots from live confocal imaging of VAP DKO cells showing juxtaposition of the *trans*-Golgi marker ST-mRFP with Rab7-EGFP (D) and Rab5-EGFP (E) positive endosomes (the mRFP and EGFP signals, which are acquired sequentially, are slightly shifted due to the high motility of the organelles). The retromer subunit VPS29-mCh colocalizes with scattered vesicles that are positive for the *trans*-Golgi marker GalT-EGFP (F), but shows no overlap with the *cis*/medial-Golgi GFPGOLPH3 that remains concentrated in the Golgi (G). Scale bar, 10 μm.

(H–J) (H) Immunofluorescence of internalized (1 hr) anti-CI-MPR antibody (pseudo colored). The internalized antibody is enriched in the perinuclear region corresponding to the TGN in WT cells, but remains disperse in peripheral puncta in VAP DKO cells (note those outside the squares). Scale bar, 10 μm. (I) Western blots of WT and VAP DKO cells revealing no major change of CI-MPR expression levels. (J) Ratio between the punctate fluorescence outside and inside squares (10×10 μm^2) centered on the Golgi complex area (see dashed squares) (n = 55 for WT and 57 for DKO cells, two-tailed t test).
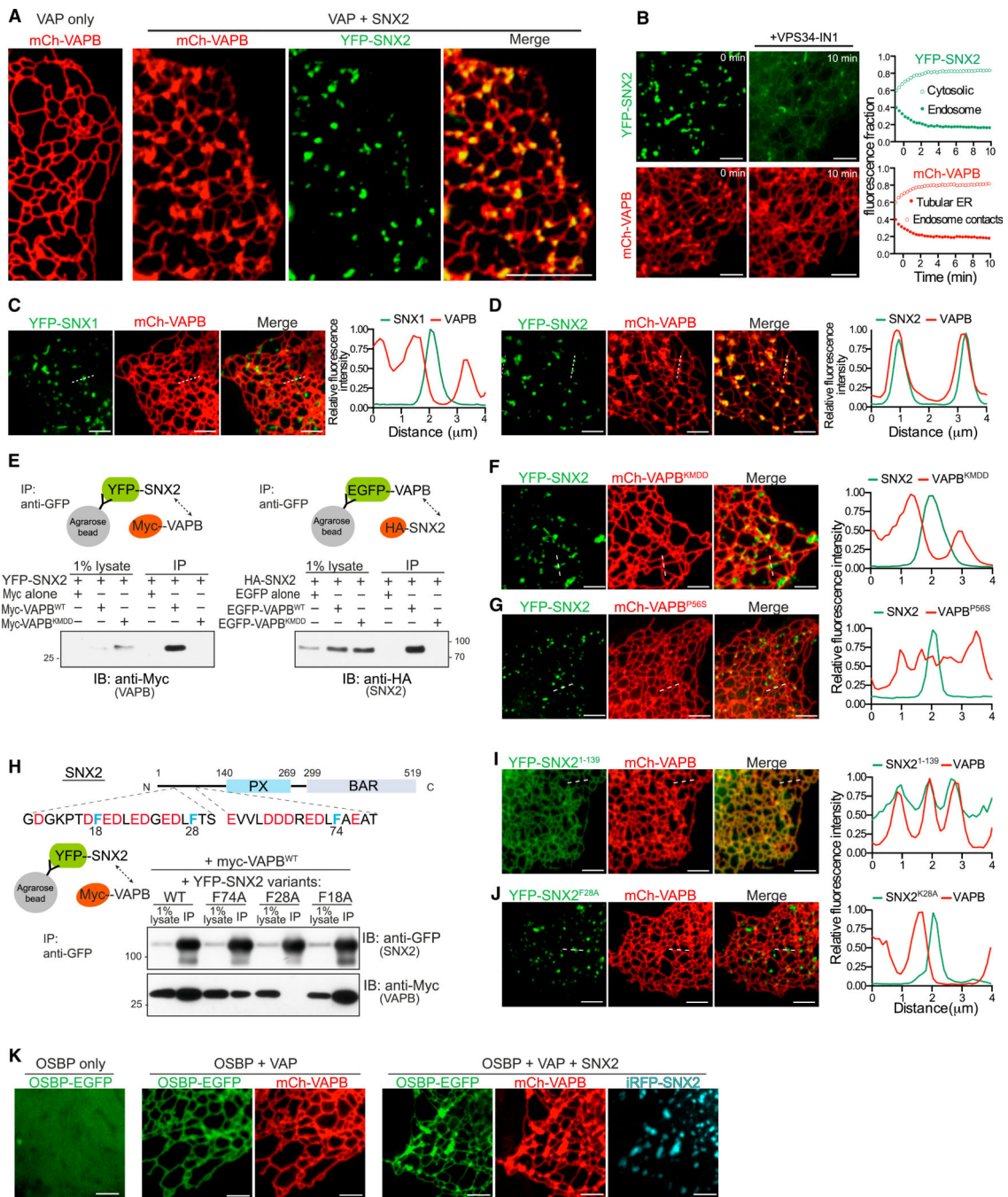
See also Figure S3.

Figure 4. Endosome-ER Tethering via an SNX2-VAPB Interaction

(A) Confocal images of COS-7 cells expressing mCh-VAPB alone, or co-expressing YFP-SNX2 and mCh-VAPB, showing the enrichment of mCh-VAP at YFPSNX2-positive endosomes. Scale bar, 10 μm.

(B) Confocal images of a COS-7 cell co-expressing YFP-SNX2 and mCh-VAPB upon treatment with the VPS34 inhibitor VPS34-IN1 (1 μM). The dissociation of YFP-SNX2 from endosomes correlates with the dispersal of mCh-VAPB throughout the ER. Quantification is shown at right. Scale bar, 5 μm. See also Movie S2.

(C and D) Confocal images and line scan analysis of COS-7 cells overexpressing YFP-SNX1 and mCh-VAPB (C), or YFP-SNX2 and mCh-VAPB (D), showing that mCh-VAPB coclusters selectively with YFP-SNX2 but not with YFP-SNX1. Scale bar, 5 μm.

(E) Extracts of HeLa cells transfected with the constructs indicated were subjected to anti-GFP immunoprecipitation (IP) and then processed for SDS-PAGE and immunoblotting (IB) with anti-Myc or anti-HA antibodies.

(F and G) Confocal images and line scan analysis of COS-7 cells co-expressing YFP-SNX2 and either the FFAT motif-binding-deficient mutant mCh-VAPB^{KMDD} (double mutant *K87D M89D*) (F), or the ALS8 mutant mCh-VAPB^{P56S} (G), showing that mCherry fluorescence remains diffuse throughout the ER tubular network and does not cocluster with YFP-SNX2. Scale bar, 5 μm.

(H) Top: SNX2 domain structure. Note the presence of sequences containing phenylalanine residues and acidic amino acids. Bottom: extract of HeLa cells transfected with myc-VAPB^{WT} and WT or mutant YFP-SNX2 were subjected to anti-GFP immunoprecipitation (IP) and then processed for SDS-PAGE and immunoblotting (IB) with anti-GFP and anti-Myc antibodies.

(I and J) Confocal images and line scan analysis of COS-7 cells co-expressing mCh-VAPB and either YFP-tagged N-terminal fragment of SNX2 (YFP-SNX2$^{1–139}$) (I), or YFP-SNX2^{F28A} (J). YFP-SNX2$^{1–139}$, which lacks the endosome binding sites but contains the FFAT-like motif, colocalizes with VAPB throughout the ER. YFP-SNX2^{F28A} localizes to endosomes but fails to cocluster with VAPB. Scale bar, 5 μm.

(K) Confocal images of COS-7 cells showing that OSBP-EGFP has a predominant diffuse localization when overexpressed alone, is recruited to the ER membrane when co-overexpressed with mCh-VAPB, and is also co-enriched with mCh-VAPB at iRFP-SNX2-positive hotspots when coexpressed with both these proteins. Scale bar, 5 μm.
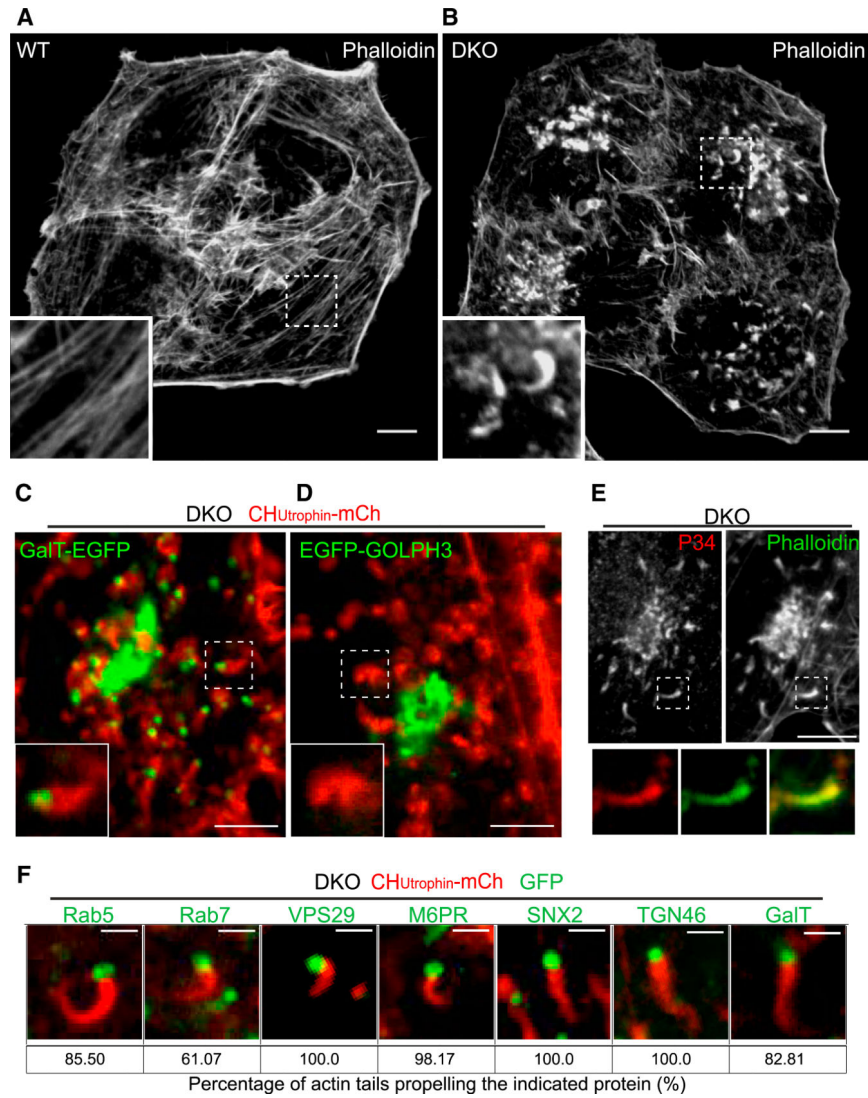
See also Figure S4.

Figure 5. Drastic Perturbation of Actin Organization in VAP DKO Cells

(A and B) Phalloidin staining of WT and VAP DKO cells showing loss of stress fiber and accumulation of actin comets in DKO cells. Insets: high magnification of the regions enclosed by dashed boxes. Scale bar, 10 μm.

(C and D) Confocal images of DKO cells showing presence of a *trans*-Golgi marker GalT-EGFP (C), but not of a *cis*/medial-Golgi protein EGFP-GOLPH3 (D), at the tips of actin comets visualized by $CH_{Utrophin}$-mCh. Insets show actin comets at high magnification. Scale bar, 10 μm.

(E) Colocalization of Arp2/3 (p34-Arc subunit) immunofluorescence and phalloidin staining in VAP DKO cells. Scale bar, 10 μm.

(F) Confocal images of DKO cells showing presence of endosomal Rabs (Rab5-EGFP; Rab7-EGFP), retromer subunits (YFP-VPS29 and YFP-SNX2), the retromer cargo GFP-CD-M6PR and *trans*-Golgi markers (TGN46-GFP, GalT-EGFP) at the tips of actin tails visualized by $CH_{Utrophin}$-mCh. Scale bar, 2 μm. Numbers below the micrographs indicate the percentage of actin tails propelling the indicated protein (n = 200 from ten cells for

Rab5, n = 131 from eight cells for Rab7, n = 99 from six cells for VPS29, n = 109 from ten cells for CD-M6PR, n = 82 from five cells for TGN46, n = 64 from four cells for GalT). See also Figure S5 and Movie S3.
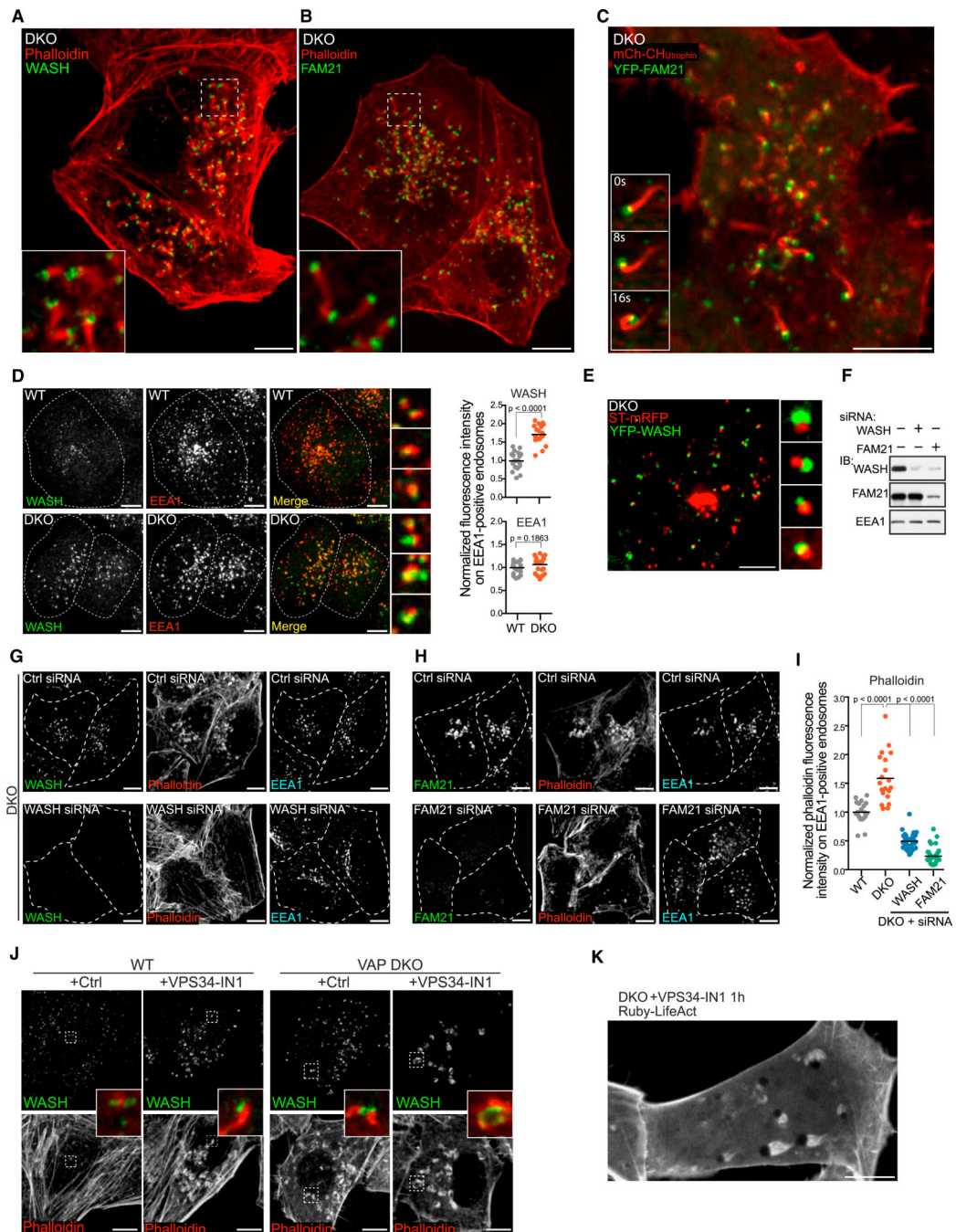
Figure 6. Actin Comets in VAP DKO Cells Are Nucleated by WASH

(A and B) WASH (A) and FAM21 (B) immunofluorescence at tips of actin tails visualized by phalloidin staining in VAP DKO cells. Scale bar, 10 μm.

(C) Live confocal images of a VAP DKO cell expressing YFP-FAM21 and the actin marker CH$_{UTR}$-mCh. Insets show at high magnification a time series of an actin comet tail propelling a FAM21-positive vesicle. Scale bar, 10 μm. See also Movie S4.

(D) Enhanced abundance of WASH on EEA1-posotivie endosomes in DKO cells (as quantified at right, n = 20 cells for each genotype, two-tailed t test). Scale bar, 10 µm. Merged images of high magnification views of individual endosomes are shown at right.

(E) Confocal image (high-magnification gallery at right) of a VAP DKO cell showing apposition of EGFP-WASH and of the *trans*-Golgi marker ST-mRFP. Scale bar, 10 µm.

(F) Western blot proving KD of WASH and FAM21. Note that FAM21 KD results in a concomitant loss of WASH.

(G–I) Phalloidin staining and immunofluorescence of DKO cells transfected with the indicated siRNAs, showing that loss of WASH (G) and FAM21 fluorescence (H) correlates with the loss of actin foci (comets) on endosomes. Scale bar, 10 µm. The normalized phalloidin fluorescence on EEA1-positive areas is quantified in (I).

(J) WASH immunofluorescence and phalloidin staining of WT and DKO cells treated with the VPS34 inhibitor VPS34-IN1 (1 µM) or solvent control (DMSO). VPS34-IN1 induces an increase of WASH and actin at the endosomal surface of both WT and DKO cells. Scale bar, 10 µm.

(K) Confocal image of VAP DKO cells expressing actin probe Ruby-LifeAct treated with VPS34 inhibitor VPS34-IN1 (1 µM) for 1 hr, showing dramatically exaggerated actin tails propelling strikingly enlarged endosomes. Scale bar, 10 µm.
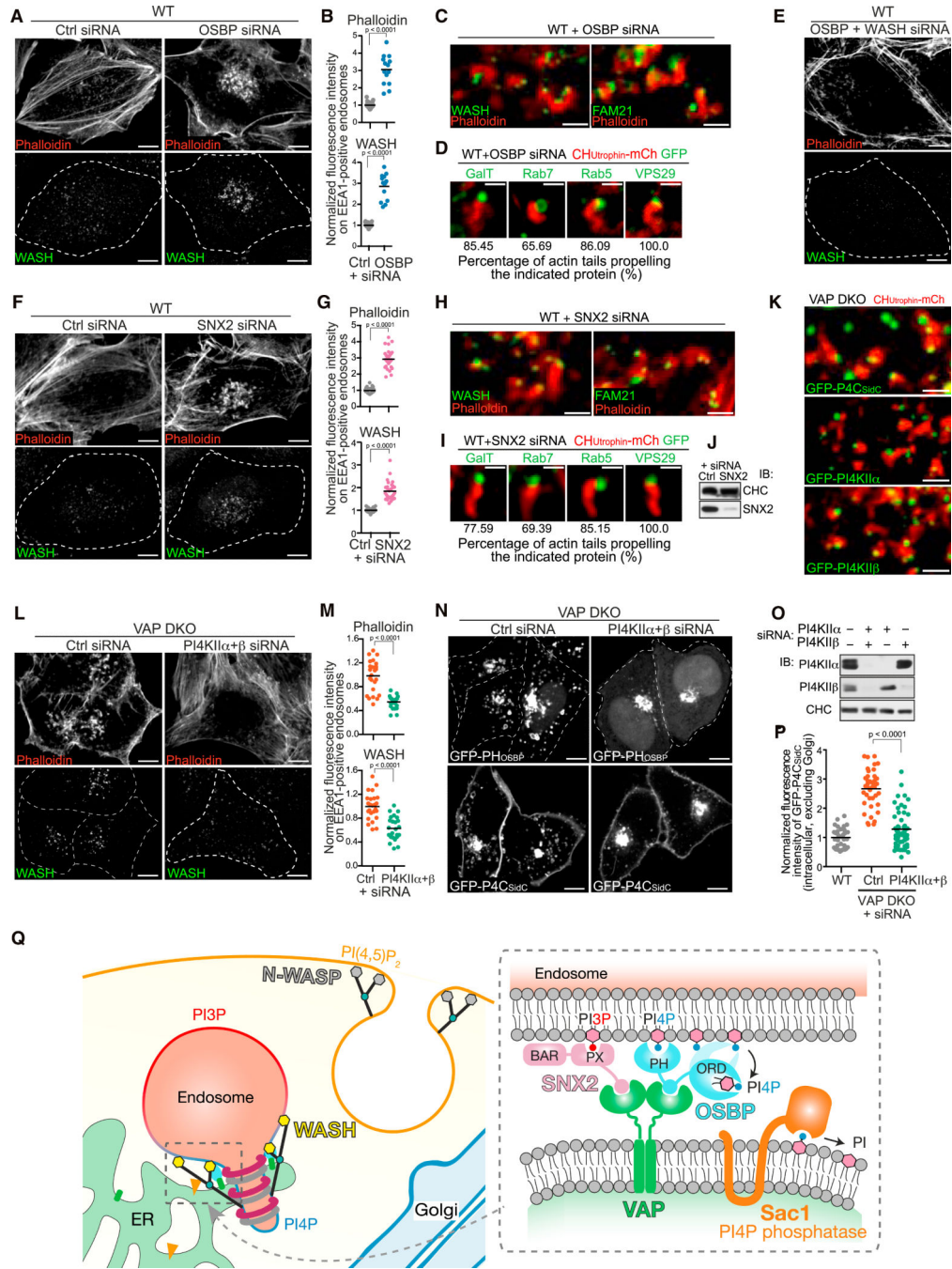
See also Figure S6 and Movie S5.

Figure 7. A Protein Network Involving Type II PI 4-Kinases and the VAP Interactors OSBP and SNX2 Is Implicated in WASH-Dependent Actin Comets Formation

(A and B) Increased abundance of assembled actin (phalloidin) and WASH immunofluorescence on intracellular organelles in OSBP KD cells (A). Scale bar, 10 μm. Normalized fluorescence intensity of WASH and phalloidin on the region occupied by EEA1-positive endosomes (see Figure S7G) is quantified in (B) (n = 20 cells for either control or OSBP siRNAs, two-tailed t test).

(C) WASH and FAM21 immunofluorescence at the tips of actin tails visualized by phalloidin staining in OSBP siRNA-treated cells. Scale bar, 2 μm. See also Movie S6.

(D) Live confocal images of OSBP siRNA-treated cells showing presence of endosomal Rabs (Rab5-EGFP; Rab7-EGFP), retromer subunits (YFP-VPS29), and a *trans*-Golgi marker (GalT-EGFP) at the tips of actin tails visualized by CH_{UTR}-mCh. Scale bar, 2 μm. Numbers below each image indicate the percentage of actin tails propelling the indicated proteins (n = 115 from seven cells for Rab5, n = 93 from five cells for Rab7, n = 99 from five cells for VPS29, n = 110 from eight cells for GalT).

(E) Immunofluorescence of WASH and phalloidin staining in WT cells transfected with OSBP and WASH siRNA, showing that loss of WASH fluorescence correlates with the loss of actin foci. Scale bar, 10 μm.

(F and G) (F) Increased abundance of assembled actin (phalloidin) and WASH immunofluorescence on intracellular organelles in SNX2 knockdown cells. Scale bar, 10 μm. Normalized fluorescence intensity of WASH and phalloidin on the region occupied by EEA1-positive endosomes (see Figure S7H) is quantified in (G) (n = 20 cells for either control or SNX2 siRNAs, two-tailed t test).

(H) WASH (left) and FAM21 (right) immunofluorescence at the tips of actin tails visualized by phalloidin staining in SNX2 siRNA-treated cells. Scale bar, 2 μm.

(I) Live confocal images of SNX2 siRNA-treated cells showing presence of endosomal Rabs (Rab5-EGFP; Rab7-EGFP), retromer subunits (YFP-VPS29), and *trans*-Golgi markers (GalT-EGFP) at the tips of actin comets visualized by CH_{UTR}-mCh. Scale bar, 2 μm. The percentage of actin tails whose tips are positive for the indicated proteins is shown under each image (n = 101 from six cells for Rab5, n = 114 from six cells for Rab7, n = 97 from five cells for VPS29, n = 116 from seven cells for GalT).

(J) Western blotting confirming the knockdown of SNX2 in WT cells.

(K) Live confocal images showing presence of the PI4P probe GFP-P4C$_{SidC}$, GFP-PI4KIIα, and GFP-PI4KIIb at the tips of actin tails in VAP DKO cells. Scale bar, 2 μm. See also Movie S7.

(L and M) Loss of assembled actin (phalloidin) and WASH immunofluorescence on intracellular organelles in VAP DKO cells upon PI4KIIs knockdown (L). Scale bar, 10 μm. Normalized fluorescence intensity of WASH and phalloidin on the region occupied by EEA1-positive endosomes (see Figure S7I) is quantified in (M) (n = 25 cells for either control or PI4KIIs siRNAs, two-tailed t test).

(N–P) Loss of PI4P on endosomal vesicles in PI4KIIs knockdown cells, as examined by two distinct PI4P probes, GFP-PH$_{OSBP}$ and GFP-P4C$_{SidC}$ (N). Western blotting confirms the knockdown of PI4KIIα and PI4KIIβ in DKO cells (O). Quantification of the normalized fluorescence of GFP-P4C$_{SidC}$ is shown in (P) (WT n = 36 cells; DKO n = 40 cells for control siRNA, and n = 50 for PI4KIIs siRNA, two-tailed t test).

(Q) Schematic illustration of ER contacts that regulate WASH-dependent actin nucleation on endosomes and retromer-dependent budding by regulating PI4P. A pool of PI4P is synthesized on endosomes by type II PI4Ks. VAP, an ER protein that forms dimers and oligomers, contributes to ER-endosome tethers via its binding to the retromer subunit SNX2 and to OSBP, which binds PI4P on the endosomal membrane via its PH domain. OSBP, via its ORD domain, makes PI4P accessible to the ER-anchored inositol 4-phosphatase Sac1. In WT cells, a transient accumulation of PI4P on endosomes is coupled to a transient burst of WASH-dependent actin nucleation to facilitate retromer function. In cells that lack VAP, loss

of PI4P downregulation results in excessive and persistent PI4P accumulation and actin nucleation on endosomes and in disruption of retromer-dependent budding.